Journal of Superconductivity and Novel Magnetism (2020) 33:3377–3393
https://doi.org/10.1007/s10948-020-05618-8

ORIGINAL PAPER

Structural, Magnetic, and Electrical Properties of $Bi_{1.6}Pb_{0.4}Sr_2Ca_2Cu_3O_{10+x}$ Superconductor Prepared by Different Techniques

A. Coşkun[1,2] · G. Akça[3] · E. Taşarkuyu[1,2] · Ö. Battal[1] · A. Ekicibil[3]

Received: 9 June 2020 / Accepted: 20 July 2020 / Published online: 1 August 2020

Abstract
In present work, we investigated the structural, magnetic, and electrical properties of $Bi_{1.6}Pb_{0.4}Sr_2Ca_2Cu_3O_{10+x}$ superconductor prepared by using four different techniques: (i) solid-state (A), (ii) sol-gel (B), (iii) chemical wet (C), and (iv) melt-quench (D). From x-ray diffraction (XRD) and transmission electron microscopy (TEM) results, it is observed that the sintering process does not influence final crystallite size of compounds, but final crystallite sizes of the compounds were nearly the same after sintering process, while initial crystallite sizes were found to be different after the preparation process. From the XRD results, it is seen that the main phase in the compound is low-T_c Bi-(2212) phase and all samples contain a small amount of high-T_c Bi-(2223) phase. From scanning electron microscopy (SEM), two different types of surface crystallization of the compounds have been observed. The low-temperature resistivity, $R(T)$, measurements show that all compounds have low zero resistivity, $T_{c,offset}$, value. Samples A, B, and C show the high-T_c and low-T_c transition at 110 and 75 K, respectively, while sample D displays only low-T_c transition at 75 K. These results have been supported by magnetization versus temperature measurement, $M(T)$. In order to calculate critical current, J_c, values for the samples, magnetic hysteresis curves were taken at temperatures 10, 20, 30, 40, 50, and 60 K between the fields of ± 9 T. The hysteresis and the J_c calculation results show that sample D, when compared with other samples, has the best superconducting properties and has the highest J_c value. The best superconductivity properties between the studied samples have been obtained for sample A, while the best magnetic properties and the highest J_c value have been observed for sample D. According to the results obtained in this study, the structural and superconducting properties change with sample preparation method.

Keywords Bi-based superconductors · Critical current density · Magnetization · TEM · XRD · SEM

1 Introduction

Bi-based superconductor (BSCCO) was discovered around 1988 [1], and those materials have been investigated extensively in recent years. The BSCCO superconductor family contains three phases having the generalized chemical formula $Bi_2Sr_2Ca_{n-1}Cu_nO_{2n+4+x}$ where $n = 1$, 2, and 3 (where n is referring to the number of CuO_2 layers in the crystal structure which responsible 20, 85, and 110 K superconducting phases, respectively) [2–3]. The formation of the high-temperature phase (2223) in BSCCO systems strongly depends on the preparation technique, sintering conditions (such as temperature, time, and heat treatment atmosphere), crystal defects, and impurity phases [4–6]. The high-T_c phase (2223 $T_c = 110$ K) is difficult to prepare in a pure form since it usually finds together with the Bi-(2212) ($T_c =$ 85 K) phase [7]. Enhancement of the transition temperature and critical current density of superconductors are very important both in scientific manner and technological application. Moreover, the reaction kinetics of the Bi-(2223) phase formation is very slow [8, 9]. Pb is mostly used as a dopant to enhance the zero resistance transition temperature and volume fraction of the high-T_c phase [10]. It has been observed that the

✉ A. Coşkun
coskunatilla@gmail.com

[1] Department of Physics, Faculty of Sciences, Mugla Sitki Kocman University, Mugla, Turkey

[2] Magnetic Materials Laboratory, Research Laboratories Center, Mugla Sitki Kocman University, Mugla, Turkey

[3] Department of Physics, Faculty of Sciences and Letters, Çukurova University, Adana, Turkey

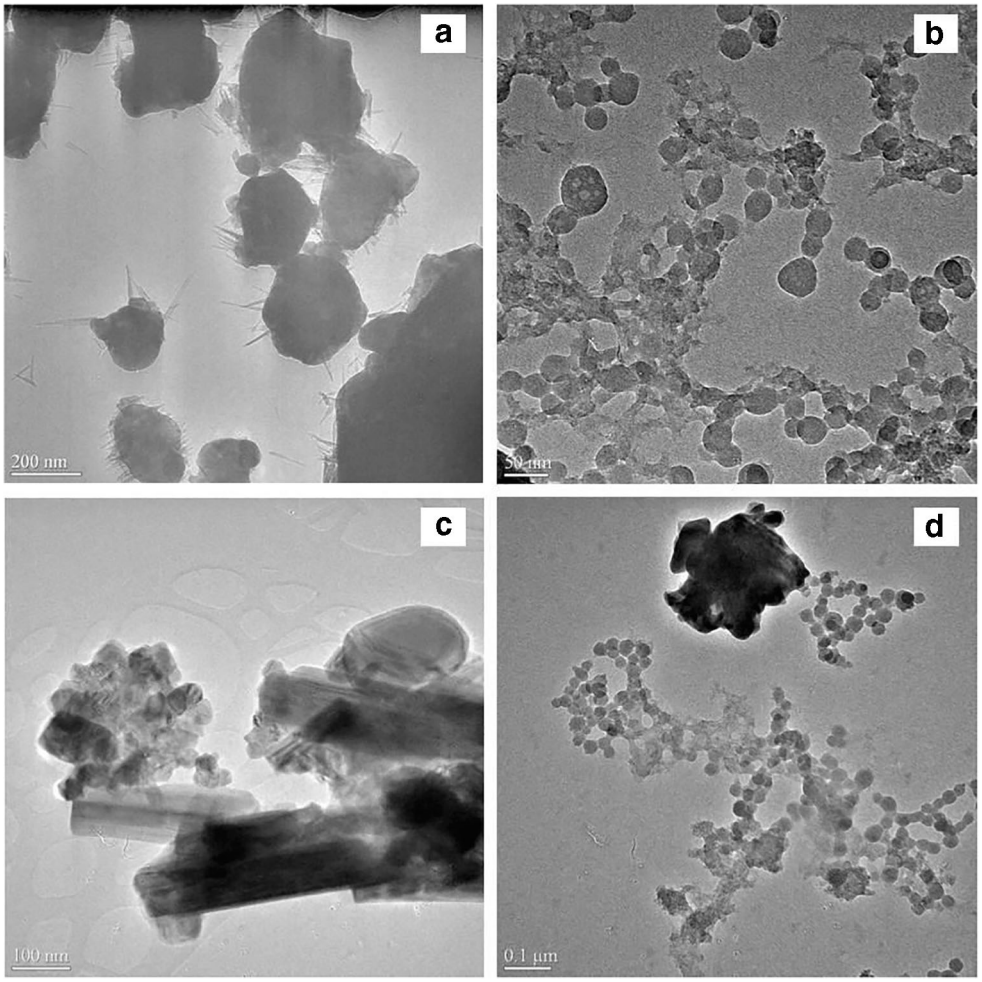

Fig. 1 TEM images before heat treatment for A, B, C, and D samples

partial substitution of Pb atoms instead of some Bi atoms supports the growth of the Bi-(2212) and Bi-(2223) phases, and a more stable compound is formed due to the small amount of Pb substitution [11, 12]. In addition to these, it is found that the melting temperature of the compounds becomes lower as a result of Pb substitution. With heat treatment under controlled conditions, the material can be prepared as a single Bi-(2223) phase. Finally, it shows a sharp T_c and zero resistivity at 110 K.

In the literature, there are different approaches related to the formation of the Bi-(2223) phase [13–15]. The most acceptable approximation of the formation of the Bi-(2223) phase is the combination of both (2212) phase that formed at between 750 and 800 °C during the sintering process and the partially melted liquid Ca_2PbO_4 phase which formed above at 820 °C [11, 16–18]. In order to confirm the validity of this approximation, the sintering temperature effects on electrical properties of Bi-based superconductors prepared by different techniques have been studied by different groups [11, 16, 18]. It is known that the superconducting properties of the compounds are affected also by the preparation techniques and the quality of the starting materials [6, 19]. To prepare Bi-based superconductors, several techniques such as solid-state reaction, melt-quench, sol-gel, chemical wet, and thin film are used generally [6–7, 19–22]. In this work, we have prepared $Bi_{1.6}Pb_{0.4}Sr_2Ca_2Cu_3O_{10+x}$ superconductor by using different production methods and studied their influences on the structural, electrical, and magnetic properties.

2 Experimental Procedure

$Bi_{1.6}Pb_{0.4}Sr_2Ca_2Cu_3O_{10+x}$ compound has been prepared by using four different ways. The details of these methods are summarized as following for solid-state, sol-gel, chemical wet and melt-quench, respectively.

Solid-State Reaction Method Appropriate amounts of starting oxides and carbonates of the respective elements (Bi_2O_3, $SrCO_3$, CaO, CuO, and PbO) were mixed, ground in programmable agate mortar for an hour, and then calcinated at 700 °C in air. The calcinated material was slowly cooled to room temperature and was ground in an agate mortar for an hour

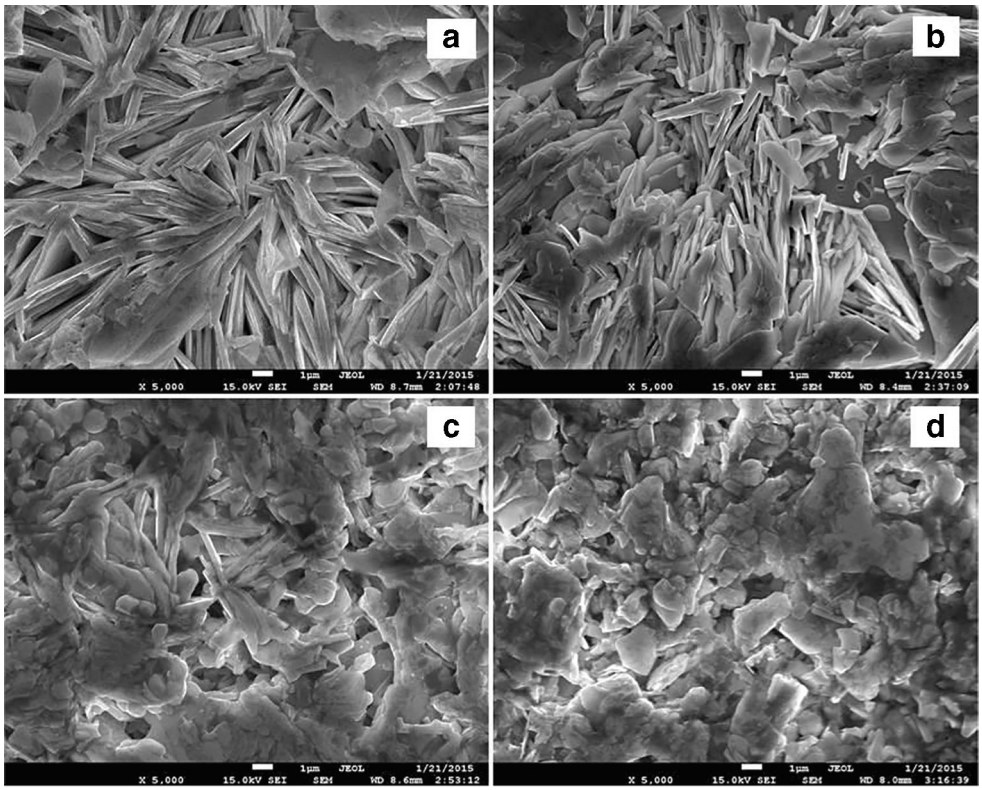

Fig. 2 SEM images taken 5kx magnification for the samples

again. This process was repeated for several times until obtained a well homogeneous mixture.

Sol-Gel Method Stoichiometric amounts of Bi_2O_3, PbO, $SrCO_3$, $CaCO_3$, and CuO were dissolved in dilute HNO_3 solution at 150 °C. Then, citric acid and ethylene glycol were added to the mixture for achieving a homogeneous solution. To obtain the viscous residual, the solution has been heated at 200 °C. The obtained residual was dried slowly at 300 °C until dry gel was formed. Finally, the precursor material was burned in the air at 600 °C in order to remove the organic materials produced during chemical reactions. The material from this process was ground to obtain a fine powder.

Chemical Wet Method In this method, the required amounts of Bi_2O_3, PbO, $SrCO_3$, $CaCO_3$, and CuO powders are mixed in a glass beaker. Then, an appropriate amount of ammonium nitrate is added into the mixed powder in the ratio of 1:1. The mixture was heated by stirring at about 180–200 °C. During the stirring, the mixture was converted to liquid form, and it is observed that some poison exhaust gases such as CO_2, NO_2, and N_2O while chemical reaction occurs. Finally, it obtained a black-like residual powder bottom of glass beaker at the end of the stirring period.

Melt-Quench Method The starting materials Bi_2O_3, PbO, $SrCO_3$, CaO, and CuO were mixed in the stoichiometric values of the nominal compositions. The materials were calcinated at 400 °C and grounded. Then, the sample was placed in a programmable furnace at room temperature, and to obtain the melted form, the sample was heated at 1200 °C in a platinum crucible. The melted sample was poured onto a precooled copper plate and pressed quickly by another cooper plate to obtain approximately 1.5 to 2 mm thickness of plate-like amorphous material. The material has been grounded for 1 h in order to obtain powder sample.

The powder materials synthesized by using four different techniques were calcinated at 750 °C for 20 h in air. The calcinated materials were grounded, and the final samples were pressed into pellets of 13 mm diameter by applying a pressure of 225 MPa. All samples were sintered at 830 °C for 100 h in air atmosphere. The samples prepared by using solid-state, sol-gel, chemical wet, and melt-quench method have been entitled as A, B, C, and D, respectively.

The morphological and crystallographic properties were investigated by SEM, TEM, and XRD techniques. The $R(T)$ measurements were carried out by a standard four-point probe in the 10–320 K range, using a closed cycle helium cryostat from Cryo Industries. The temperature dependence of the magnetization ($M(T)$) were measured using a Quantum Design PPMS superconducting quantum interference device magnetometer with VSM (vibrating sample magnetometer) head.

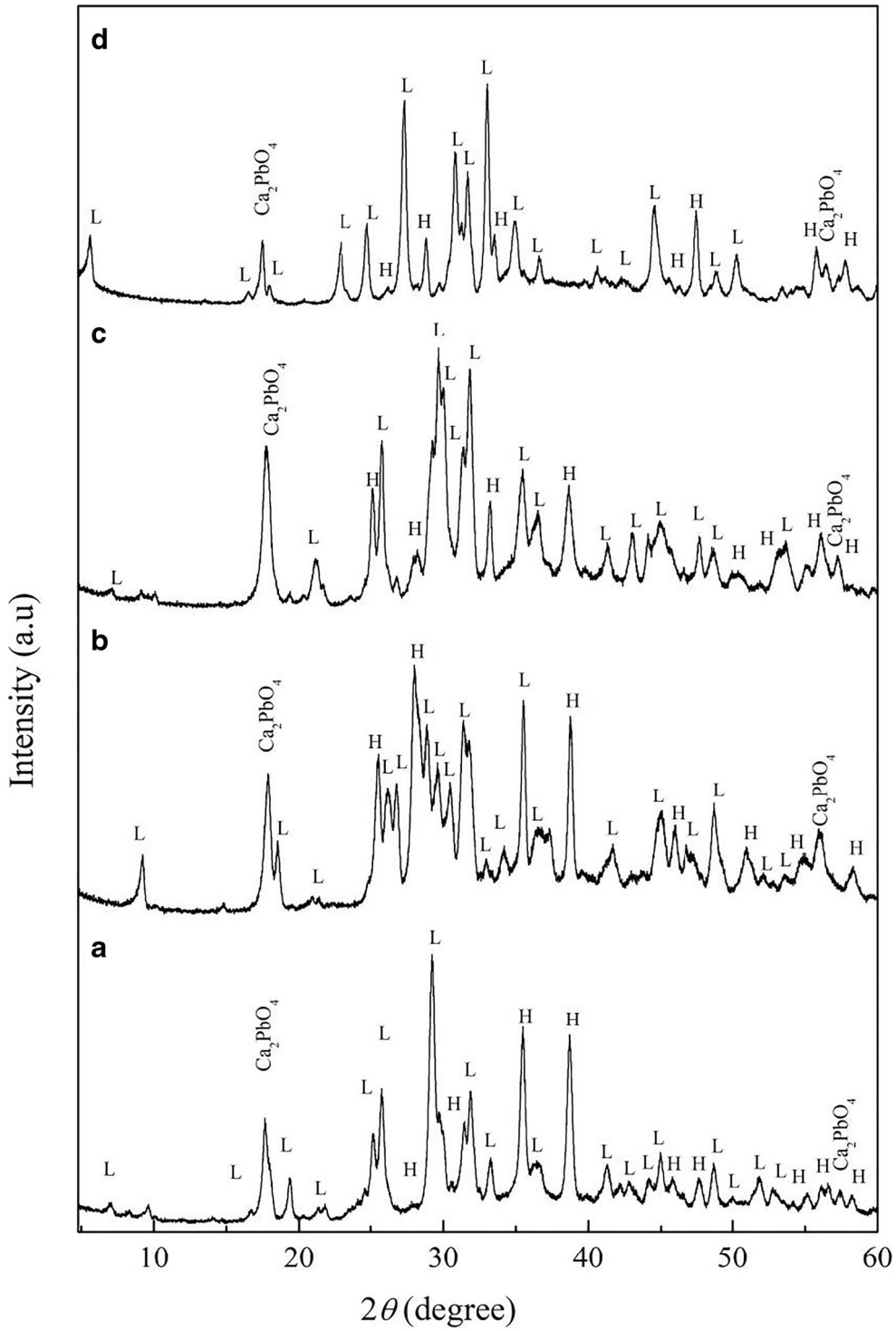

Fig. 3 The XRD patterns of samples A, B, C, and D

Table 1 The percentage of the Bi-(2223) and Bi-(2212) and Ca_2PbO_4 phases for the samples

Sample	Bi-(2223) (%)	Bi-(2212) (%)	Ca_2PbO_4 (%)
A	28.9	66.6	4.5
B	21.3	73.9	4.8
C	19.6	74.5	5.9
D	16.6	77.2	6.2

Table 2 $T_{c,onset}$, $T_{c,offset}$, and ΔT values of the samples

Sample	$T_{c1,onset}$ (K)	$T_{c2,onset}$ (K)	$T_{c,offset}$ (K)	ΔT (K)
A	110	75	64	46
B	110	75	62	48
C	110	75	59	51
D	–	75	55	20

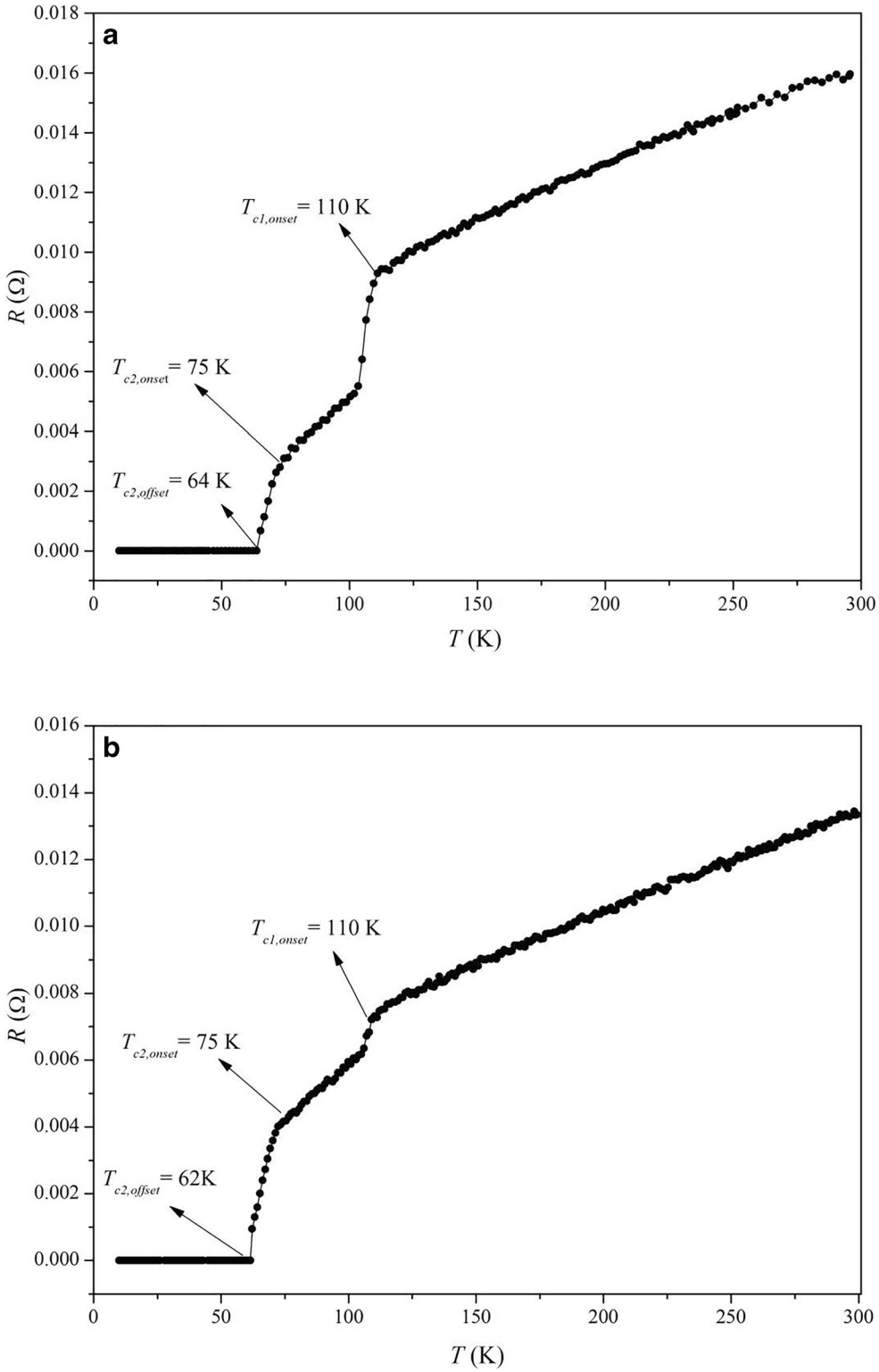

Fig. 4 $R(T)$ curves of samples A, B, C, and D

3 Results and Discussion

Figure 1 a–d show TEM images of the A, B, C, and D samples prepared by different production methods before heat treatment. As seen in Fig. 1a, sample A has consisted of randomly distributed needlelike formation at the edge of the crystallites. The crystallite size for sample A changes between 0.2 and 0.5 μm. The shape of crystallites for sample B is spherical, and the crystallite sizes vary between 20 and 50 nm (see Fig. 1b). From the TEM image of sample C, two different kinds of

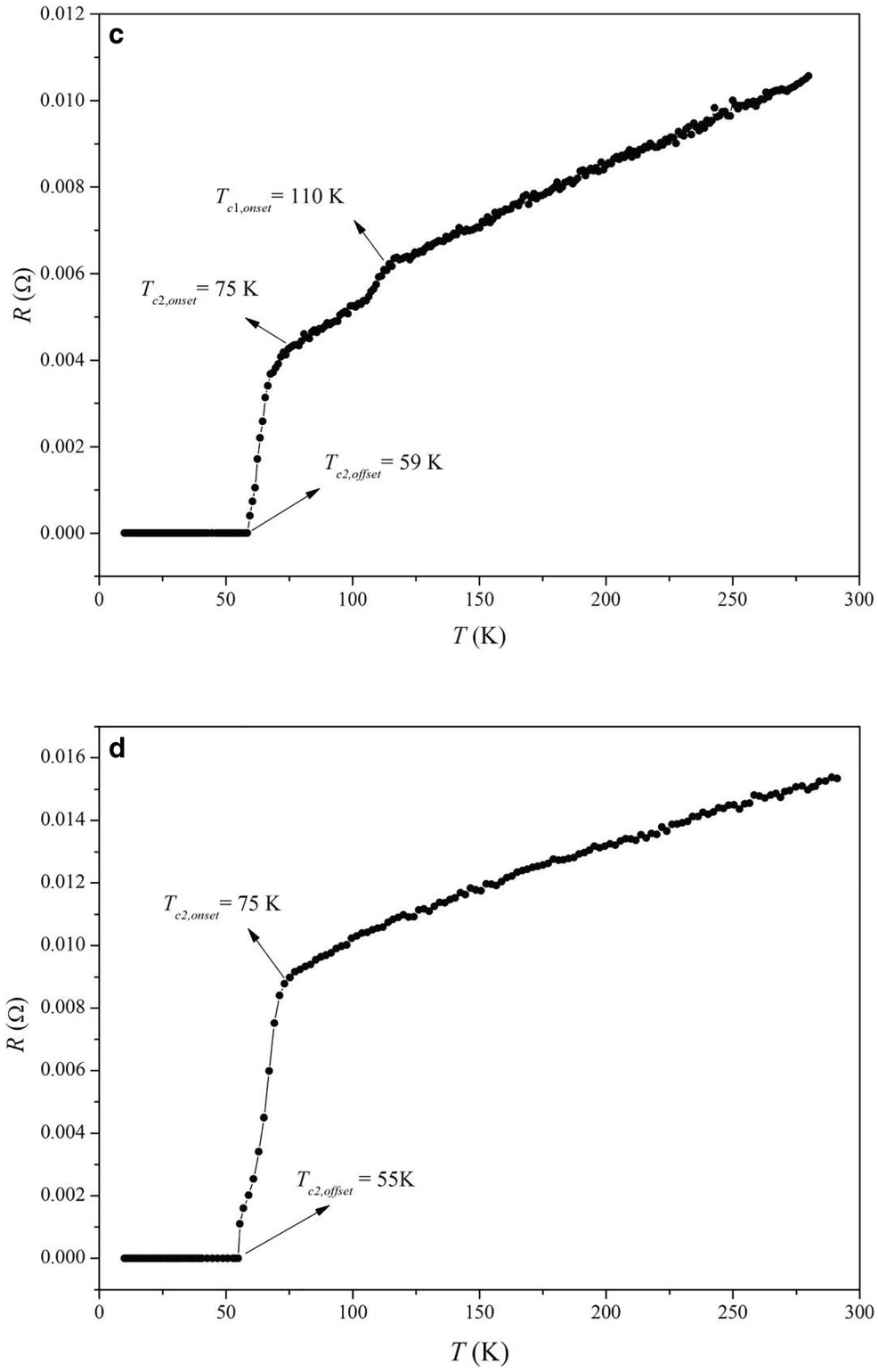

Fig. 4 (continued)

grain formation are seen. One of them is clusters that were formed by a combination of small grains whose size is smaller than 100 nm, and the other is long rectangular bars whose size is much greater than the other (> 500 nm). The TEM image of sample D is given in Fig. 1d. It is seen clearly that the compound form from the chains of nano-sizes (20–50 nm) spherical small grains and a cluster of large grain that sizes change between 0.5–1 μm. It is seen from the TEM images that the

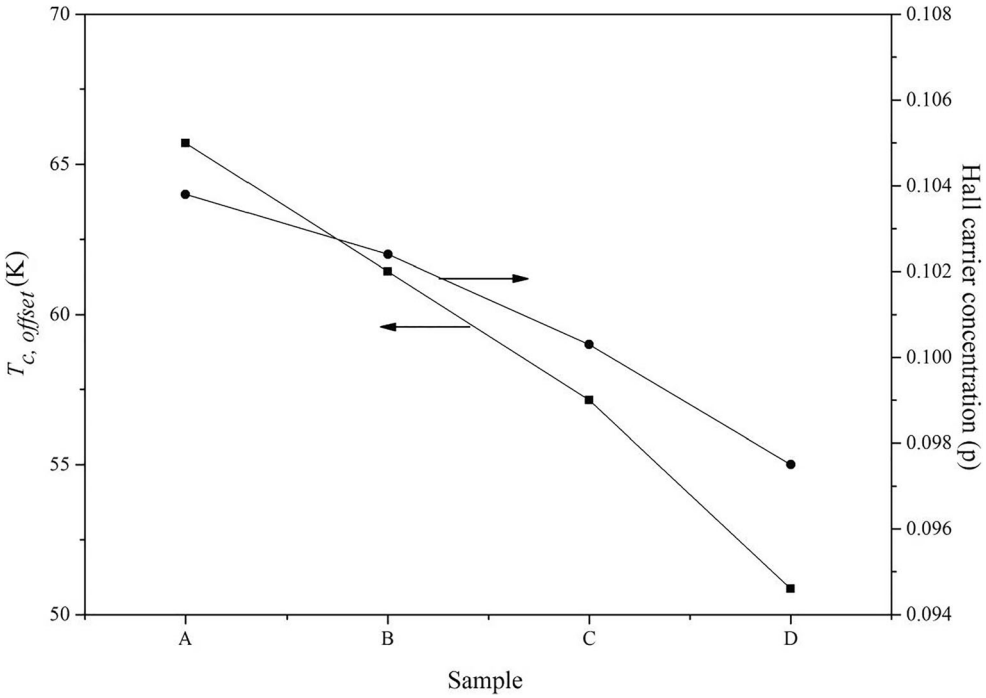

Fig. 5 Hall carrier concentration and the $T_{c,offset}$ values of samples A, B, C, and D

grain sizes of the samples are different from each other. This may arise from the presence of some impurities observed in the structure by depending on the preparation techniques.

In order to get information about crystallization, surface morphology, and the grain size of the compounds after the sintering process, SEM photographs were taken 5kx magnifications. The SEM images of the samples are shown in Fig. 2a–d. It is observed that there are two different kinds of grain formation on the surface morphology for the A sample (see Fig. 2a). A well-connected the twiggy structure which is composing perpendicular to the surface has been observed and planar grains have formed also under and above of the twiggy grains in the structure. In addition to these different formations for the A sample, there is some porosity between twiggy regions. The number of these grains is greater than that of the planar ones, but their grain size is also smaller. It is observed that the surface crystallization of sample B is similar to sample A (see Fig. 2b). But, the sizes and the number of the twiggy grains are less than that of sample A. It can be said that the formation of the twiggy grains is the initial state. Occurrences of the twiggy grains on the surface of the samples state that the high-T_c 2223 phases have just started the forms in the structure. Figure 2 c–d) show the SEM images of the C and D samples. The surface morphologies of C and D samples are different. The formation of the planar structure on the surface increased, while the formation of twiggy grains decreased. According to the results, the size, shape, and distribution of the grains of all samples are different from each other. According to results, the different sample production techniques affect the surface morphology of the samples.

Figure 3 shows that the XRD patterns of the A, B, C, and D samples were taken at room temperature. It is seen from XRD patterns of the samples that all samples contain the Bi-(2212), Bi-(2223), and Ca_2PbO_4 impurity phase. The volume fractions of the Bi-(2212), Bi-(2223), and Ca_2PbO_4 impurity phases for the samples were determined by using the following expressions [23]:

$$\mathrm{Bi{-}(2223)\%} = \frac{\sum I(2223)}{\sum I(2223) + \sum I(2212) + \sum I(\mathrm{Ca_2PbO_4})} \quad (1)$$

$$\mathrm{Bi{-}(2212)\%} = \frac{\sum I(2212)}{\sum I(2223) + \sum I(2212) + \sum I(\mathrm{Ca_2PbO_4})} \quad (2)$$

$$(\mathrm{Ca_2PbO_4})\% = \frac{\sum I(\mathrm{Ca_2PbO_4})}{\sum I(2223) + \sum I(2212) + \sum I(\mathrm{Ca_2PbO_4})} \quad (3)$$

Bi-(2223)% and Bi-(2212)% represent the integrated intensity of Bi-(2212) and Bi-(2223), respectively. The percentage of Ca_2PbO_4 impurity phases is given as Ca_2PbO_4%. The percentages of these phases for all samples are given in Table 1. According to Table 1, Bi-(2212) phase is dominant for all samples, and Bi-(2212) phase has not transformed into the Bi-(2223) phase. Bi-(2223) peaks start to occur nearly next to the characteristic Bi-(2212) peaks for all samples. But, the characteristic peak ($2\theta = 39.3°$) belonging to Bi-(2223) phase has been observed in only sample A. The presence of wide

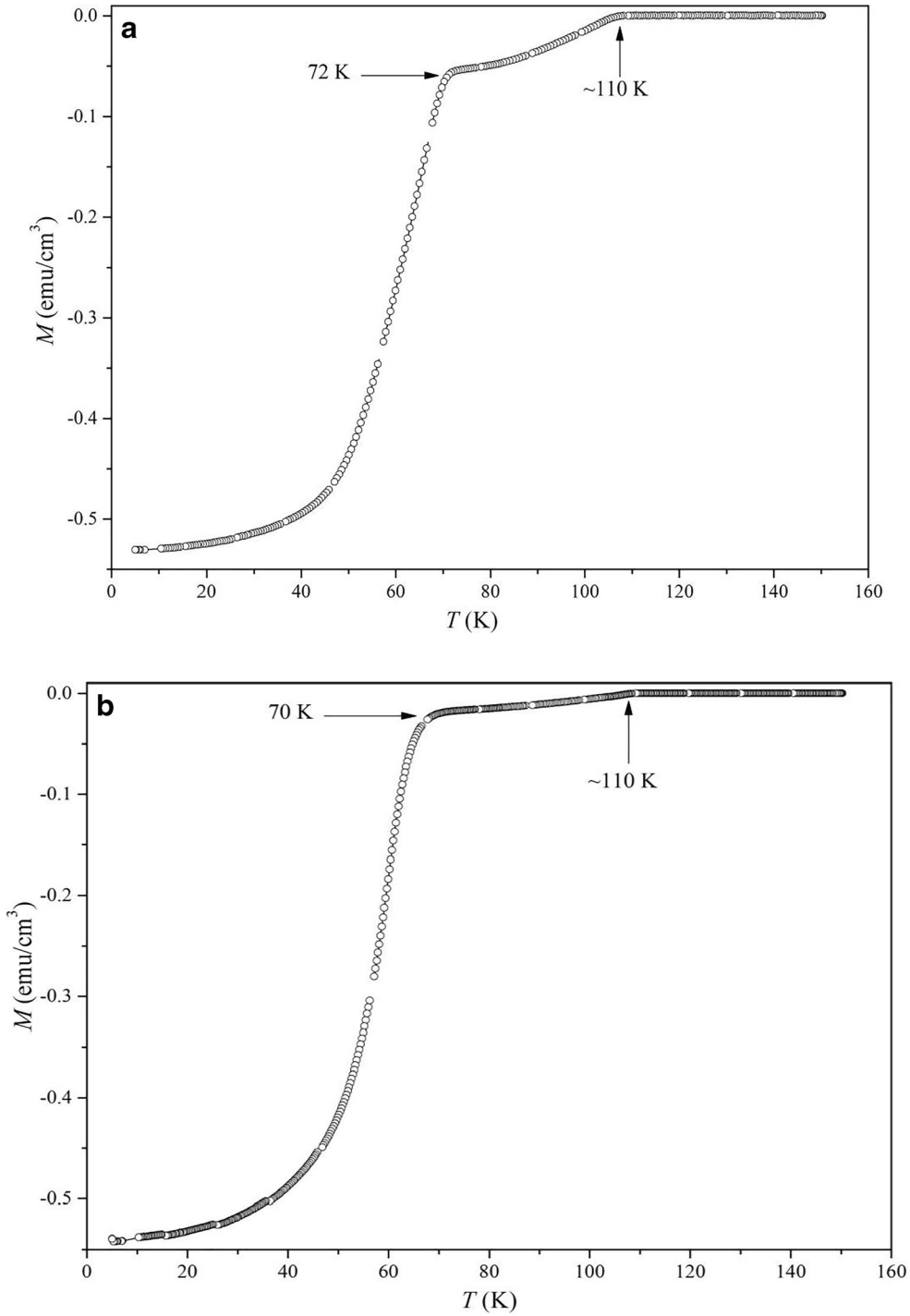

Fig. 6 The $M(T)$ curves for samples A, B, C, and D

diffraction peaks seen from the XRD patterns of all samples expresses that the formation of the Bi-(2223) phase is not completed during sintering process and the heat treatment temperature chosen to obtain the Bi-(2223) phase is not sufficient. It is known that substitution of Bi ions by Pb ions causes the formation of the Bi-(2223) phase and increases T_c value of the new compound (optimum lead content lies between 0.3 and 0.4) [24, 25]. Also, Pb-doped Bi-based superconductors contain Ca_2PbO_4 or PbO impurity phases which occur during the heat treatment, and these phases play a crucial role in the formation of the high-T_c phase [26]. Many studies showed that the high-T_c (2223) phase is formed via combining low-T_c (2212) and Ca_2PbO_4 impurity phases [27–28]. All compounds which are studied in this study contain Ca_2PbO_4 impurity phases. In Table 2, the percentages of the Bi-(2223) and Bi-(2212) and Ca_2PbO_4 phases for the samples are given.

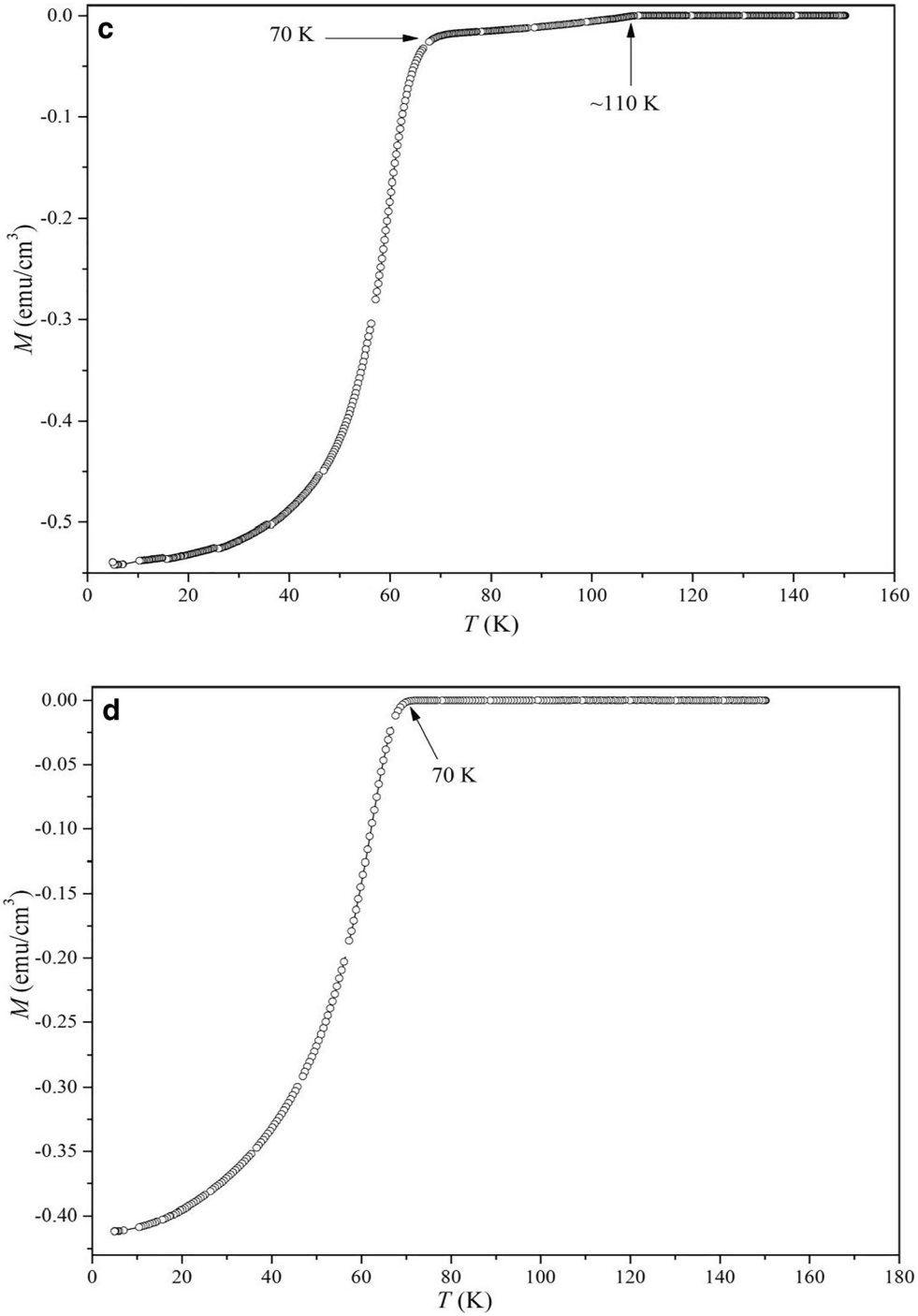

Fig. 6 (continued)

The ratio of Bi-(2212) and Ca_2PbO_4 phases is highest for the D sample when compared with that of others. This may change the electrical properties of the samples.

The average crystallite size (D) was calculated by using Debye–Scherrer formula which is defined like [29]:

$$D = \frac{\kappa \lambda}{\beta cos\theta} \quad (4)$$

where λ is the x-ray wavelength, β is the line broadening at full width at half maximum height (FWHM), θ is the Bragg angle, and κ is a constant related to crystallite shape, normally taken as 0.9. The crystallite size of the samples was found to be 204.7 Å, 203.1 Å, 207.8 Å, and 202.6 Å for samples A, B, C, and D, respectively. It found different crystallite sizes for the compounds from TEM images (see Fig. 1a–d) that were

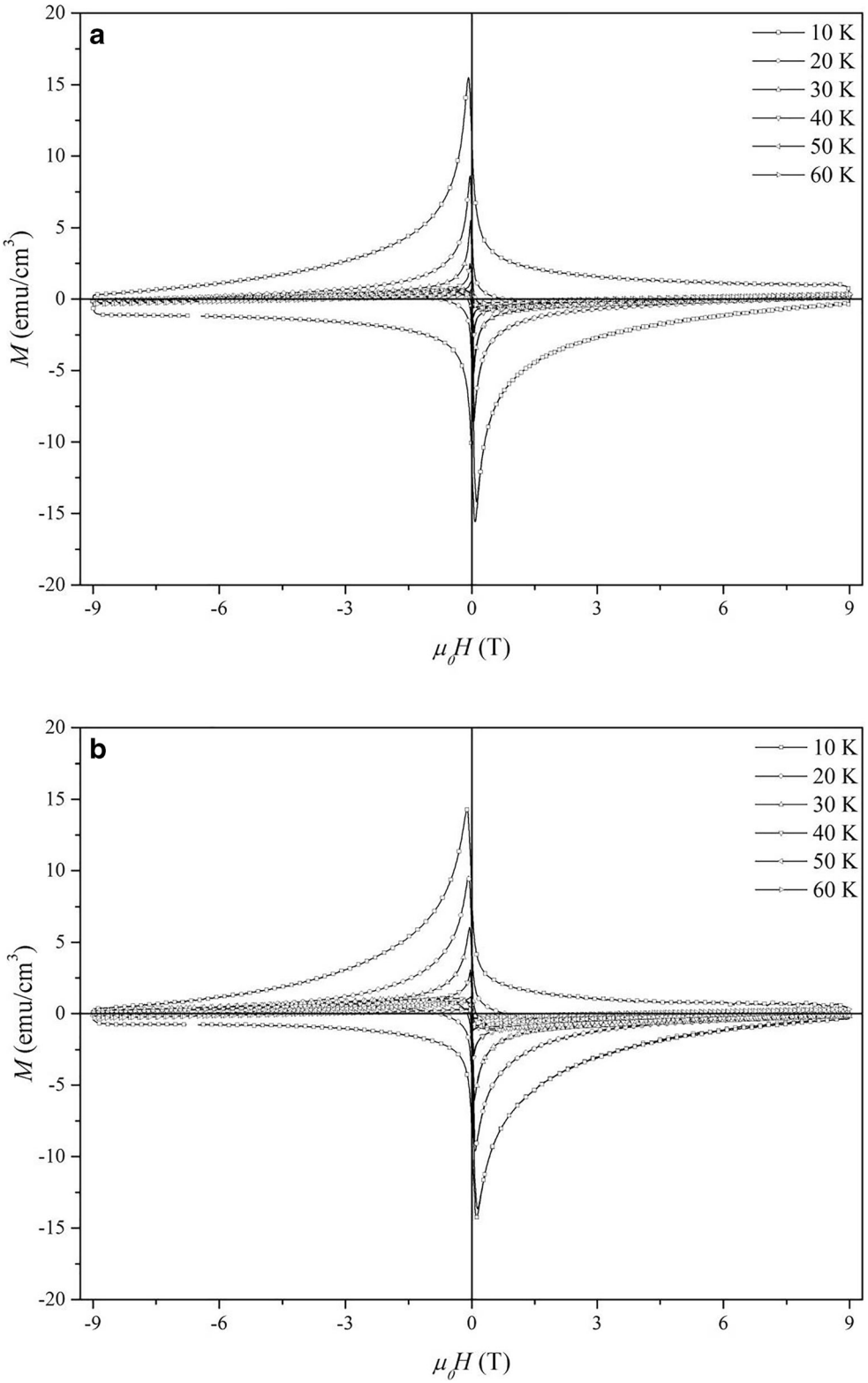

Fig. 7 The $M(H)$ curves of the samples at 10, 20, 30, 40, 50, and 60 K

taken before heat treatment. However, as can be seen from the calculations, all compounds have almost the same crystallite sizes after the heat treatment although they were produced by different production techniques.

In order to investigate the superconducting behavior and determine the transition temperature of the compounds, the temperature dependence of resistivity measurements, $R(T)$, have been performed at 10–300 K temperature interval under

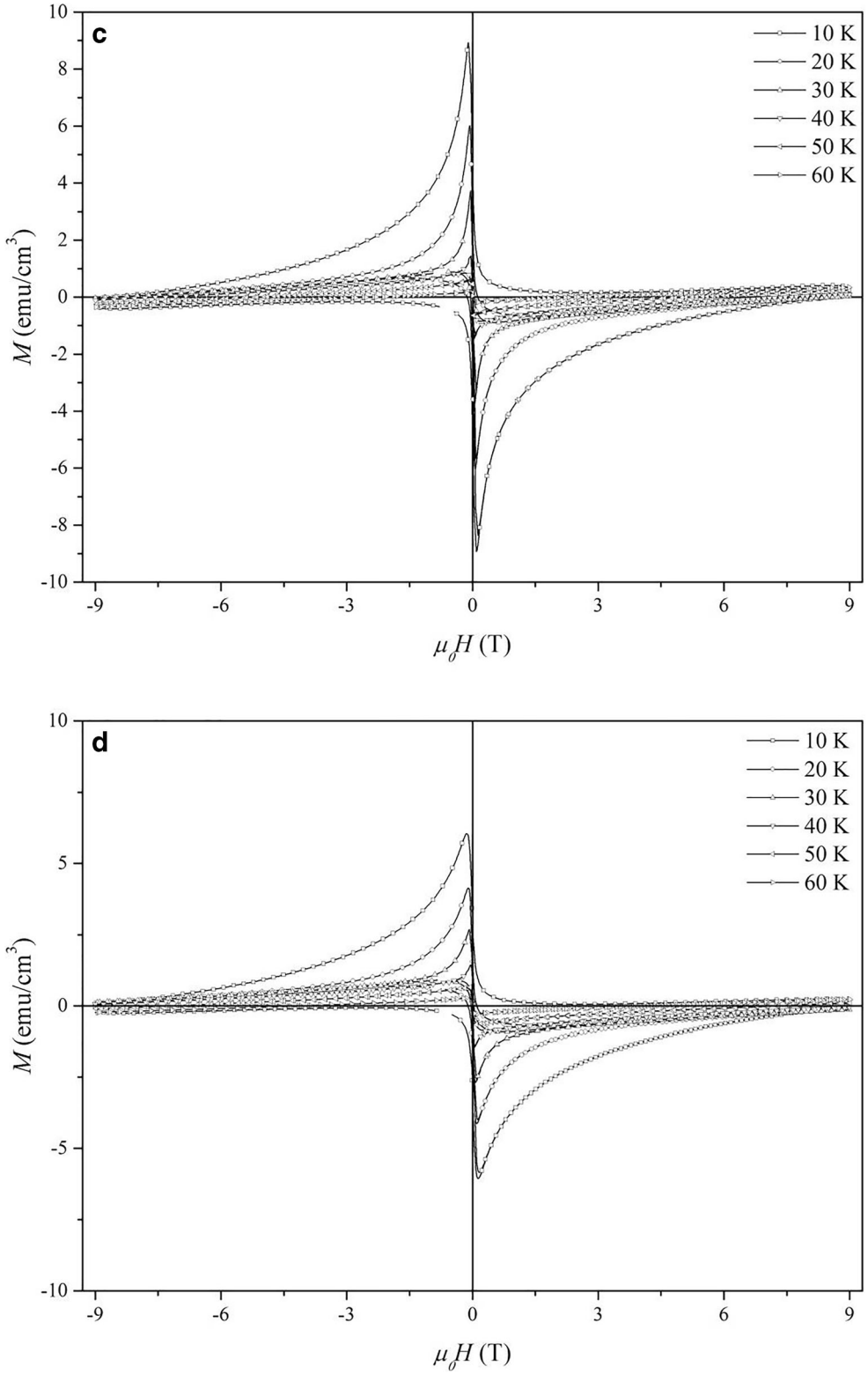

Fig. 7 (continued)

zero magnetic field. Figure 4 shows the $R(T)$ curves of the samples. It is clearly seen from Fig. 4 that the samples display characteristic metallic behavior at temperatures 300–110 K interval K. Two onset transition temperatures, $T_{c,onset}$, were observed at temperatures of about 110 and 75 K which are most likely due to the presence of both the high-T_c and low-T_c

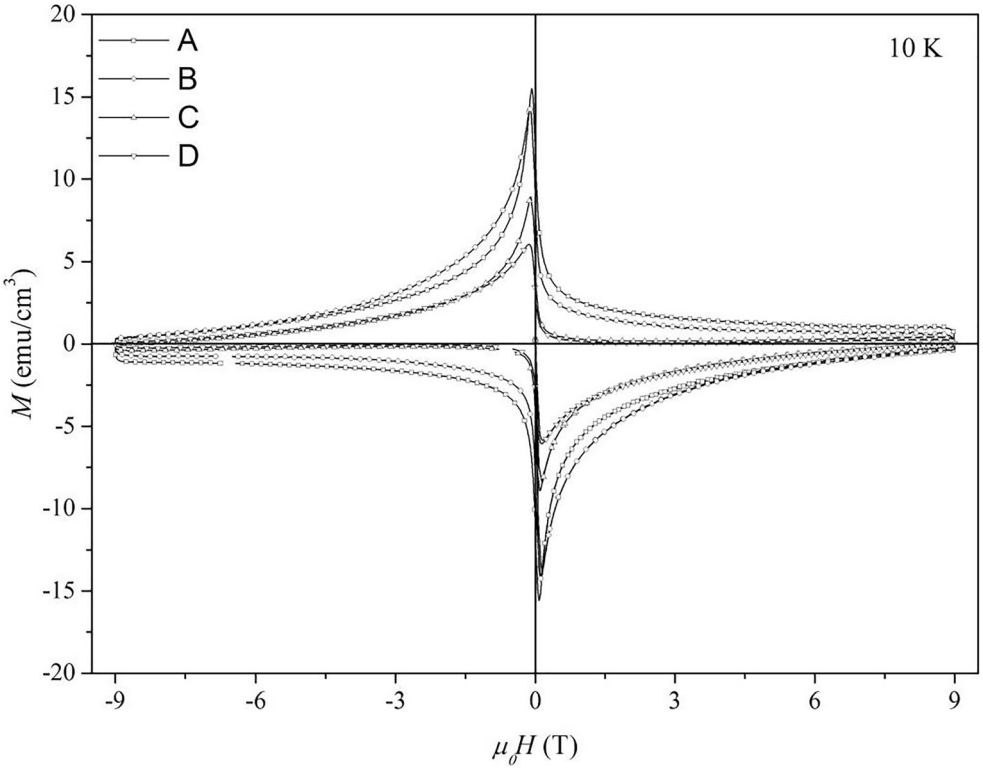

Fig. 8 Magnetic hysteresis curves of the samples at 10 K

phases in samples A, B, and C, while sample D has only low-T_c phase at 75 K. Although the $T_{c,onset}$ value is 110 K, R goes to zero at $T_{c,offset}$ at 64, 62, and 59 K for samples A, B, and C, respectively (see Table 2). There is a big difference between $T_{c,onset}$ and $T_{c,offset}$ value ($\Delta T = T_{c,onset} - T_{c,offset}$) of the samples, and this represents that the Bi-(2212) is the dominant for all samples. This result corresponds with XRD result and the ratio of Bi-(2212) phase.

By using the $R(T)$ results, we have also calculated to the hall carrier concentration (P) per Cu ions of the sample due to the following relation [30]:

$$P = 0.16 - \left[\frac{\left(1 - \frac{T_{c,\ offset}}{T_{c,onset}}\right)}{82.6}\right]^{1/2} \quad (5)$$

Figure 5 shows the relation between hall carrier concentration and the $T_{c,offset}$ values of the samples. It is seen that the samples in both hall carrier concentration and the $T_{c,offset}$ values have the same trend and sample A has the maximum P values as $T_{c,offset}$.

Figure 6 shows the magnetization measurements as a function of temperature ($M(T)$) of samples A, B, C, and D in the range of 5–150 K and in an applied magnetic field of 0.01 T. It is clearly seen that sample A exhibits a diamagnetic behavior (first critical transition temperature) below 110 K. Meanwhile, it has the second critical transition temperature in the $M(T)$ curve which occurred near 72 K. In general, this kind of behavior arises from the different phase formations in the sample. The critical transition temperature values are very close to the $T_{c,onset}$ and $T_{c,offset}$ values of the A, B, and C samples which were found from the $R(T)$ measurements. However, sample D has only one critical transition temperature which occurs nearly at 70 K. The $M(T)$ curve represents that sample D has only Bi-(2212) as well as it was found from XRD and $R(T)$ measurements.

Magnetic hysteresis cycles, $M(H)$, of the samples were performed at different temperatures (for 10, 20, 30, 40, 50, and 60 K) between the fields of ± 9 T. Figure 7 shows the $M(H)$ curves of the samples. For all samples, the hysteresis loops are symmetrical and increase with decreasing temperature. This implies the existence of the flux pinning centers [31]. The area under the hysteresis loop is proportional to the superconducting properties of the samples [8]. The area is larger at 10 K for all samples with compared to obtain at other temperatures. This result is an indicator of the existence of strong pinning center in superconductor samples at 10 K, and also these centers show strong resistance opposite of the applied magnetic field at this temperature. It is observed that the areas under hysteresis curves decreased due to the increasing temperature which represents that the strengths of the pinning centers are decreasing. The hysteresis loops which taken at 60 K have the smallest area for all samples. This behavior explained that this temperature is very close to the $T_{c,offset}$ value of the compounds.

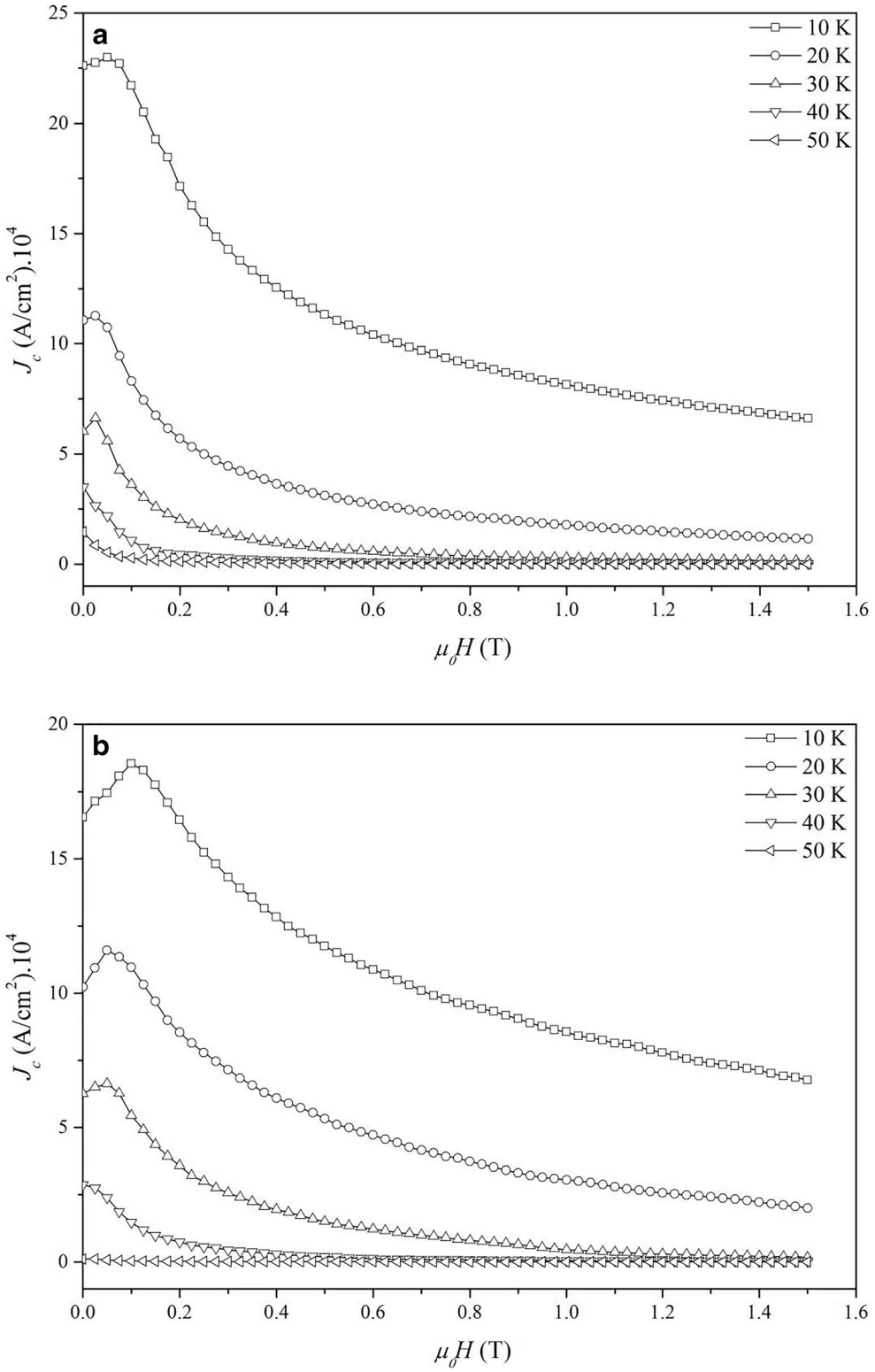

Fig. 9 The calculated critical current densities as a function of applied magnetic field for all the samples at different temperatures

In Fig. 8, the combination of the hysteresis curves of the samples which were taken at 10 K is given. We obviously see that sample A has the largest area which is result of the best superconducting properties and also the remagnet magnetization value which is the proportional the superconducting volume is the higher in all samples. This result is consistent with other measurements. The trend of the hysteresis curves is very

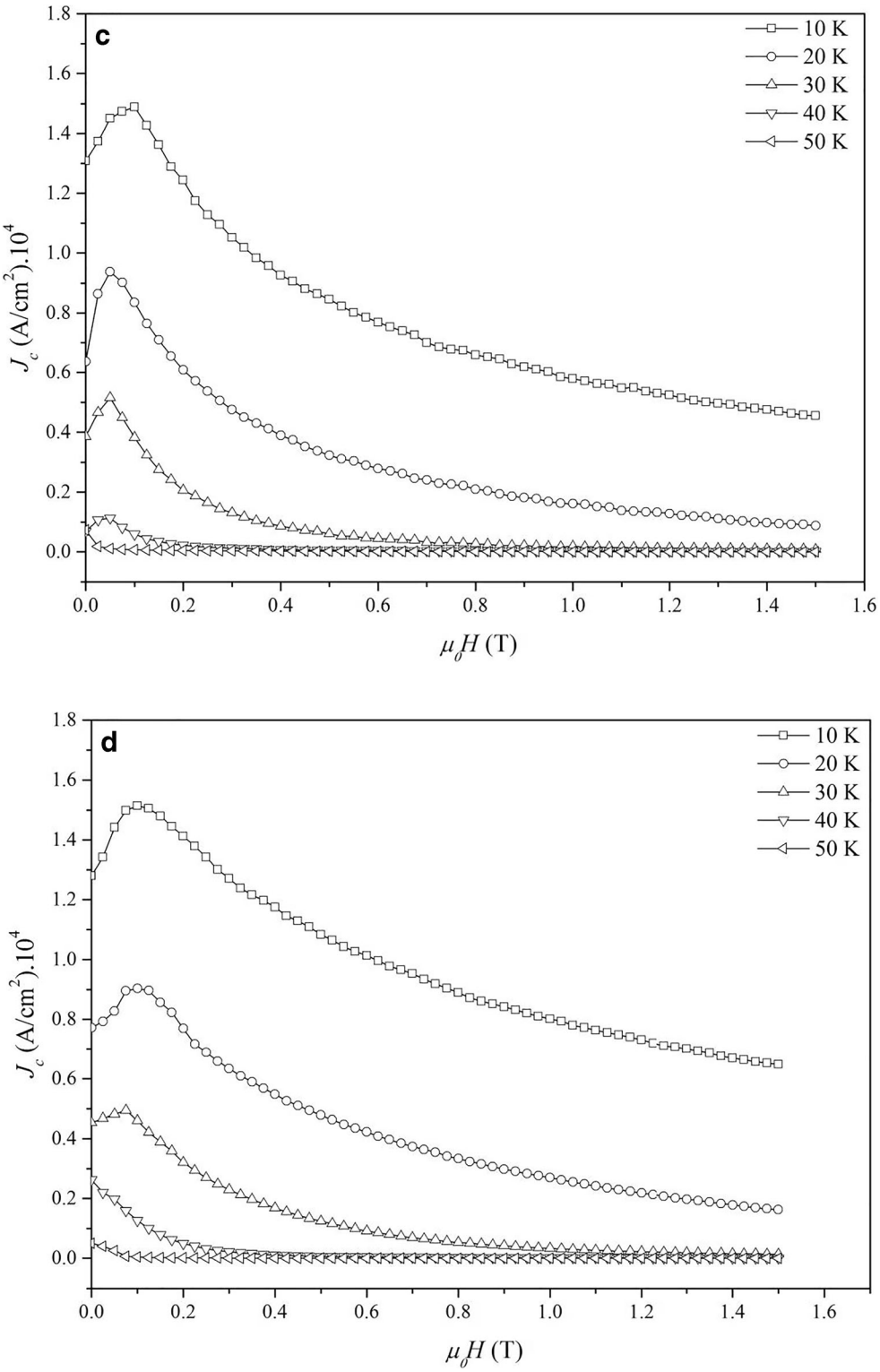

Fig. 9 (continued)

symmetrical which shows the presence of strong pinning center in the samples.

The value of the critical current density, J_c, is an important parameter for many technological applications. The value of the J_c is proportional to the area under the hysteresis curves. If this area is large enough, it means that the J_c will be a bigger value. The graphs of the J_c values versus applied magnetic fields at a certain temperature give some information about

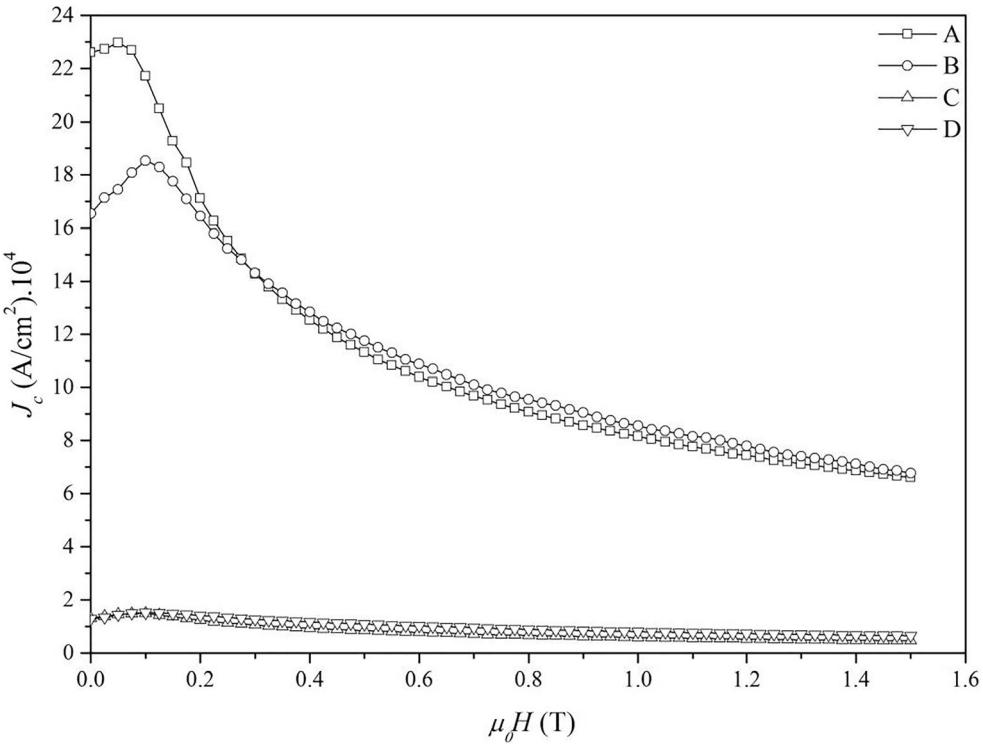

Fig. 10 The applied magnetic field dependence of the critical current densities for all samples at 10 K

the magnitude and the activity of the pinning centers. In this work, the J_c values calculated the hysteresis data which were taken at 10, 20, 30, 40, 50, and 60 K by using Bean Critical State Model [32] that relates to the $M^+$and M^- acquired from the intersection of $M(H)$ loops at a chosen applied magnetic field. The critical model formula is given as [4]:

$$4\pi(M^+ - M^-) = \left(\frac{4\pi}{10}\right) J_c \left(\frac{d}{3}\right) \tag{5}$$

where the units of $M^+$and M^- are emu/cm^3, J_c is the critical current density in A/cm^2, and d is the sample thickness in centimeters [10]. The temperature dependencies of the J_c values of the compounds are shown in Fig. 9. In all samples, a remarkable increase in J_c values which calculated at the 10, 20, and 30 K was observed up to the value at which the applied external magnetic field up to 0.1 T. It is possible to explain that kind of increase in the J_c values stem from strong pinning center and the activity of the flux tubes [33]. It is well known that the change in the applied magnetic field causes regulation of the density of flux tubes. The flux tubes can move freely in the superconducting region and their density rearrangement due to the applied magnetic field [34]. But, impurity or secondary phases, inhomogeneities in the superconductor due to the grain boundaries and also crystal lattice defects behavior like an energy wall and contributes to the improvement of the flux pinning force, results block to move of the vortices in the compounds [10]. So, the magnetic flux in the superconductors was not changed in a reversible manner as the external magnetic field changes to 0.1 T. The increase in J_c value up to 0.1 T indicates that the strong pinning center raises from the strong connection between the grain boundaries and improves the supercurrent paths which exist in the compounds [10]. A substantially rapid decrease of J_c values was observed due to the increasing temperature (20 to 60) for all samples. The low critical currents can be attributed to the poor connection between the superconducting grains due to the increasing temperature.

Figure 10 shows the applied magnetic field dependence of J_c for the compounds. It is obviously seen that sample A has higher J_c values than that of the other samples. Low-temperature resistivity measurements $R(T)$ showed that sample A has largest Bi-(2223) phase, while it has smallest Bi-(2212) and Ca_2PbO_4 impurity phase compared with other samples. Therefore, it is possible to say that the higher J_c values related to the amount of Bi-(2223) and Bi-(2212) phases in the compounds. J_c values are consistent with the volume fraction of both Bi-(2223) and Bi-(2212) phases and the impurity phase in all compounds of this study. It should be indicated that the value of J_c is almost completely related to defects in superconducting materials. Large J_c values indicate the existence of strong flux pinning in the materials [10]. By comparing the results mentioned above, one can conclude that the strong flux pinning centers are more effective in sample A.

4 Conclusion

In this study, the $Bi_{1.6}Pb_{0.4}Sr_2Ca_2Cu_3O_{10+x}$ superconductors were prepared by using four different preparation techniques, sintered at 830 °C in air atmosphere. The structural, electrical,

and magnetic properties of the compounds were investigated. The TEM results were obtained in this study, to produce nano-sized compounds, and the best method is the sol-gel. The SEM investigations showed that the surface morphology formed two different types of grin formation, twiggy and the plane like. These kinds of structural inhomogeneities which are formed in the compounds may be responsible for the lower T_c. The $R(T)$ measurements show that the samples have the multiphase superconducting structure. The $M(T)$ measurement results of the compounds support the $R(T)$ measurements of the samples. The largest hysteresis and the critical current density were observed for sample A. According to the results that were obtained in this study, one can be said that the structural, superconducting, and magnetic properties were best for sample A which are prepared by solid-state method.

Funding Information This work is supported by the Scientific Research Foundation (BAP) of Muğla Sıtkı Koçman University, Muğla, Turkey, under grant contracts no. 14/074.

References

1. H. Maeda, Y. Tanaka, M. Fukutumi, and T. Asano, Jpn. J. Appl. Phys. 27 (2) (1988)
2. Yildirim, G., Varilci, A., Terzioglu, C.: Anisotropic natüre and scaling of thermally activated dissipation mechanism in Bi-2223 superconducting thin film. J.Alloy.Compd. **554**, 327–334 (2013)
3. Dogruer, M., Yildirim, G., Varilci, A., Terzioglu, C.: MgB_2 inclusions in Bi-2223 matrix: the evaluation of microstructural, mechanical and superconducting properties of newsystem, Bi-2223+MgB_2. J. Alloys Compd. **556**, 143–152 (2013)
4. A. Ekicibil, A. Coşkun, B. Özçelik and K. Kıymaç, "Critical current densities in (x=0.01, 0.1) superconductors prepared by melt-quenching method and annealed in different time intervals ", Modern Physics Lett B, 2011
5. Mohammed, N.H., Awad, R., Abou-Aly, A.I., Brahim, I.H., Hassan, M.S.: Optimizing the preparation conditions of Bi-2223 superconducting phase using PbO and PbO_2. Mater. Sci. Appl. **3**, 224–233 (2012)
6. Tampieri, A., Celotti, G., Lesca, S., Bezzi, G., La Toretta, T.M.G., Magnani, G.: Bi(Pb)–Sr–Ca–Cu–O (2223) superconductor prepared by improved sol–gel technique. J. Eur. Ceram. Soc. **20**(2), 119–126 (2000)
7. Kharissova, O.V., Kopnin, E.M., Maltsev, V.V., Leonyuk, N.I., León-Rossano, L.M., Pinus, I.Y., Kharisov, B.I.: Recent advances on bismuth-based 2223 and 2212 superconductors: synthesis, chemical properties, and principal applications. Crit. Rev. Solid. State. Mater. Sci. **39**, 253–276 (2014)
8. A. Ekicibil, A. Coşkun, B. Özçelik, K. Kiymaç, "The effect of Gd concentration on the physical and magnetic properties of $Bi_{1.7}Pb_{0.3-x}Gd_xSr_2Ca_3Cu_4O_{12+y}$ superconductors", Journal of Low Temperature Physics 140 (2005)105–117
9. Tarascon, J.M., McKinnon, W.R., Barboux, P., Hwang, D.M., Bagley, B.G., Grene, L.G., Hull, G.W., Page, Y.L., Stoffel, N., Giroud, M.: Preparation, structure, and properties of the superconducting compound series $Bi2Sr_2Ca_{n-1}Cu_nO_y$ with n 1, 2, and 3. Phys. Rev. B. **38**(1988), 8885
10. Coşkun, A., Özçelik, B., Kıymaç, K.: Physical properties of melt-cast annealed $Bi_{1.6}Pb_{0.4}Sr_2Ca_3Cu_4O_{12}$ compound. Turk. J. Phys. **25**, 473–479 (2001)
11. Chen, Y.L., Stevens, R.: 2223 phase formation in Bi(Pb)─Sr─C─a─Cu─O: II, the role of temperature—reaction mechanism. J.Am.Ceram. Soc. **75**(5), 1150–1159 (1992)
12. Sözeri, H., Ghazanfari, N., Özkan, H., Kılıç, A.: Enhancement in the high-Tc phase of BSCCO superconductors by Nb addition. Supercond. Sci. Technol. **20**, 522–528 (2007)
13. A. Mchirgui, M. Zouaoui, F. B. Azzouz, M.A. B Said, R. Smirani, M.B. Salem, "Kinetic formation of (Bi,Pb)-2223 compound during the last stage of a multi-step thermal preparation process", Physica : Condensed Matter, Volume 321, Issues 1–4, (2002) 283–286
14. Yavuz, M., Maeda, H., Vance, L., Liu, H.K., Dou, S.X.: Phase development and kinetics of high temperature Bi-2223 phase. J. Alloys Compd. **281**(2), 280–289 (1998)
15. Garnier, V., Monot-Laffez, I., Desgardin, G.: Kinetics study of the Bi-2223 grain growth thickness. Physica C: Superconductivity Volume. **349**(1–2), 103–112 (2001)
16. Hatano, T., Katsumi, K., Ikeda, S., Nakamura, K., Ogawa, K.: Growth of the 2223 phase in leaded Bi-Sr-Ca-Cu-O system. Jpn. J. Appl. Phys. Part II. **27**, L2055–L2058 (1988)
17. Sarkar, A.K., Tang, Y.J., Cao, X.W., Ho, J.C., Kozlowski, G.: Role of calcium plumbate during the formation of 2223 phase in the Bi(Pb)SrCaCuO system. Mater. Res. Bull. **27**(1), 1–8 (1992)
18. Wang, R.K., He, Q., Yu, D.A., Di, X.X., Li, Y.H.: Structure of Bi-Pb-Sr-Ca-Cu-O superconductor with Tc of 108 K. Modern Physics Letters B. **3**(4), 341–347 (1989)
19. Li, D., Zhang, H., Gao, X., Yang, S., Chen, Q.: Effect of the fabrication process on the electrical properties of polycrystalline $Bi_{1.7}Pb_{0.3}Sr_2Ca_2Cu_3O_{10}$. Ceram. Int. **42**, 1728–1732 (2016)
20. Gul, I.H., Anis-ur-Rehman, M., Maqsood, A.: Temperature dependence of thermal and electrical conductivity of Bi-based high-Tc (2223) superconductor. Physica C. **450**, 83–87 (2006)
21. Safran, S., Ozturk, H., Bulut, F., Ozturk, O.: The influence of repelletization and heat treatment on physical, superconducting, magnetic and micro-mechanical properties of bulk BSCCO samples prepared by ammonium nitrate precipitation method. Ceram. Int. **43**, 15586–15592 (2017)
22. Akça, G., Ekicibil, A., Kiymaç, K.: Influence of lithium-holmium co-doped on structural and electrical properties of BSCCO superconductor. J. Optoelectron. Adv. Mater. **15**(3–4), 229–234 (2013)
23. Halim, S.A., Khawaldeh, S.A., Mohammed, S.B., Azhan, H.: Superconducting properties of $Bi_{2-x}Pb_xSr_2Ca_2Cu_3O_y$ system derived via sol-gel and solid state routes. Mater. Chem. Phys. **61**, 251–259 (1999)
24. Green, S.M., Jiang, C., Meiyu Luo, H.L., Politis, C.: Zero resistance at 107 K in the (Bi,Pb)-Ca-Sr-Cu oxide system. Phy. Rev.B. **38**, 5016 (1988)
25. Chavira, E., Escudero, R., Rios Jara, D., Leon, L.M.: Influence of lead on the formation of the 110-K superconducting phase in the Bi-Sr-Ca-Cu-O compounds. Phy.Rev.B. **38**(1988), 9272
26. Uzumaki, T.: Kazunori Yamanaka, Nobuo Kamehara and Koichi Niwa, "the effect of Ca_2PbO_4 addition on superconductivity in a Bi-Sr-Cu-O system". Jpn. J. Appl. Phys. **28**(1), L75–L77 (1989)
27. Biju, A., Abhilash Kumar, R.G., Aloysius, R.P., Syamaprasad, U.: Structural and superconducting properties of Bi1.7Pb0.4Sr2_xGdxCa1.1Cu2.1Oy system. Physica C. **449**, 109–115 (2006)
28. Koo, H.-S., Tseng, T.-Y.: Preparation and characteristics of Bi-Pb-Sr-Ca-Cu-O superconducting films by spray pyrolysis and post-annealing. Mater. Chem. Phys. **56**, 226–235 (1998)
29. Cullity, B.D.: Element of X-ray Diffraction. Addition-Wesley, Reading (1978)
30. Azzouz, B.F., Mchirgui, A., Yangui, B., Boulesteix, C., Salem, B.M.: Synthesis, microstructural evolution and the role of substantial addition of PbO during the final processing of (Bi, Pb)-2223 superconductors. Physica C. **356**, 83 (2001)

31. Özkurt, B., Ekicibil, A., Aksan, M.A., Özçelik, B., Yakıncı, M.E., Kıymaç, K.: Structural and physical properties of Nd substituted bismuth cuprates $Bi_{1.7}Pb_{03-x}Sr_2Ca_3Cu_4O_{12+y}$. J. Low Temp. Phys. **149**, 105–118 (2007)
32. Bean, C.P.: Magnetization of hard superconductors. Phys. Rev. Lett. **8**, 250 (1962)
33. R. Kossowsky, B. Raveau, D.Wohlleben, S. K. Patapis, "Physics and Materials Science of High Temperature Superconductors II", 1992
34. Arani, H.F., Baghshahi, S., Sedghia, A., Stornaiuolo, D., Tafuri, F., Massarotti, D., Riahi-Noori, N.: The influence of heat treatment on the microstructure, flux pinning and magnetic properties of bulk BSCCO samples prepared by sol-gel route. Ceram. Int. **44**, 5209–5218 (2018)